CONTROLLING THE ENZ PROFILE FOR BROADBAND NONRECIPROCAL THERMAL EMITTERS WITH HIGH CONTRAST BETWEEN EMISSIVITY AND ABSORPTIVITY

Changkang Du and Bo Zhao[1]

Department of Mechanical Engineering, University of Houston, Houston, TX 77204, USA

ABSTRACT. Recent advances have revealed exciting new opportunities of nonreciprocal thermal emitters for photon-mediated thermal and energy applications by breaking Kirchhoff's law of radiation. However, most nonreciprocal emitters reported can only achieve high contrast between emissivity and absorptivity in a relatively narrow frequency and angular range, limiting their wide applications. Emitters consisting of multiple semiconductor layers with different doping levels have attracted a lot of attention for the fabrication feasibility and promises for achieving broadband nonreciprocal thermal emission due to epsilon-near-zero response. However, there has not been a systematic study on how the multilayers should be arranged for optimal performance. In this work, we study the effect of doping profile on nonreciprocal thermal radiative properties. By optimizing the arrangement of the layers, we achieve a contrast of 0.6 between emissivity and absorptivity, highest contrast in this system to the best of our knowledge.

1 INTRODUCTION

Kirchhoff's law of radiation states that the emissivity equals the absorptivity for the same frequency and direction [1-3]. This equivalence between emissivity and absorptivity has been widely applied in designing thermal and energy functionalities, such as thermal camouflage [4], solar energy harvesting [5, 6], and radiative cooling [7, 8]. However, recently, it has been shown that the validity of Kirchhoff's law is rooted in Lorentz reciprocity. In systems that break reciprocity (nonreciprocal), Kirchhoff's law can be violated [9-11]. Nonreciprocal emitters has drawn great interest in many research areas, such as energy harvesting [12-14] and radiative heat transfer [15-17]. Existing designs of nonreciprocal emitters mainly use two kinds of materials, i.e., magneto-optical materials [11, 18, 19] and Weyl semimetals [9, 20, 21]. Both materials support an epsilon-near-zero (ENZ) wavelength range where the dielectric function across zero, and nonreciprocal properties can be greatly enhanced by the ENZ effect. Despite the predominant enhancement to nonreciprocal radiative properties, the enhancement effect is confined within a narrow wavelength range [22]. The narrowband nonreciprocal emission cannot meet the requirement for energy and thermal applications in which broadband nonreciprocal thermal radiation is needed.

Recently, gradient multilayer structures are proposed to address this challenge [23-25]. Each layer in these emitters has a different parameter, such as carrier concentration or chemical potential, providing a broad wavelength range in which ENZ effect can be significant. For example, Zhang and Zhu [24] propose a nonreciprocal thermal emitter using a gradient doped InSb multilayer on top of a reflector. In this structure, each layer has a different doping level to have a different ENZ wavelength, and a broadband nonreciprocity from 12 to 16 μm is achieved. In another work, Liu et al. [25] design a multilayer structure using ultrathin magnetized InAs films with different doping to enable different ENZ wavelengths, achieving a broadband nonreciprocal emission from 20 to 40 μm. The realization of broadband nonreciprocal thermal emitters is inspiring. However, it is still unclear whether the

[1] Corresponding Author: bzhao8@uh.edu.

profile of ENZ wavelengths can affect the contrast between emissivity and absorptivity for such multilayer semiconductor emitters while maintaining the broadband feature. For a linear doping profile in which the doping level difference between two adjacent layers is constant, the changing direction of the doping profile may make a difference. In addition to the linear doping profile, a nonlinear doping profile also can affect the performance of multilayer structures with gradient parameters [26]. There has not been a systematic study on how the multilayers should be arranged to have a better doping profile for optimal nonreciprocal performance.

In this work, we study the effects of doping profiles on the performance of nonreciprocal broadband multilayer semiconductor emitters. We analyze the nonreciprocal performance of linearly doped multilayer structures. We apply a nonlinear doping profile to such multilayer structures and achieve the largest contrast between emissivity and absorptivity among broadband nonreciprocal multilayer emitters with a magnetic field 1.5 T, to the best of our knowledge. Our results pave the way to achieving high-performance broadband nonreciprocal multilayer emitters.

2 METHODS AND MATERIALS

We start by introducing the method we use to compute the emissivity and absorptivity of nonreciprocal emitters. As shown in Figure 1a, a system consists of an opaque thermal emitter and two blackbodies A and B, under thermal equilibrium, with the three objects at the same temperature. From the second law of thermodynamics, part of the emission from blackbody A is absorbed by the thermal emitter, and the other part is reflected and then absorbed by blackbody B, and we have

$$\alpha_{\mathrm{A}} + r_{\mathrm{A}\to\mathrm{B}} = 1 \tag{1}$$

where α_{A} is the absorptivity in the direction A at a given wavelength, and $r_{i\to j}$ is the reflectivity of the emitter from channel *i* to channel *j* at a given wavelength, with $i, j \in \{\mathrm{A}, \mathrm{B}\}$. Similarly, follow the emission from blackbody B, we have

$$\alpha_{\mathrm{B}} + r_{\mathrm{B}\to\mathrm{A}} = 1 \tag{2}$$

Meanwhile, at thermal equilibrium, each blackbody receives the same amount of energy as it emits, which yields

$$\varepsilon_{\mathrm{A}} + r_{\mathrm{B}\to\mathrm{A}} = 1 \tag{3}$$

and

$$\varepsilon_{\mathrm{B}} + r_{\mathrm{A}\to\mathrm{B}} = 1 \tag{4}$$

Combining equation (1)-(4), we have

$$\alpha_{\mathrm{A}} - \varepsilon_{\mathrm{A}} = r_{\mathrm{BA}} - r_{\mathrm{AB}} \tag{5}$$

For reciprocal emitters, $r_{\mathrm{BA}} = r_{\mathrm{AB}}$, and therefore $\alpha_{\mathrm{A}} = \varepsilon_{\mathrm{A}}$, which is Kirchhoff's law of radiation. However, for nonreciprocal emitters, $r_{\mathrm{BA}} \neq r_{\mathrm{AB}}$, and thus $\alpha_{\mathrm{A}} \neq \varepsilon_{\mathrm{A}}$. More specifically,

$$\alpha_{\mathrm{A}} = 1 - r_{\mathrm{AB}} \tag{6}$$

and

$$\varepsilon_{\mathrm{A}} = 1 - r_{\mathrm{BA}} \tag{7}$$

The above two equations are used to compute the emissivity and absorptivity of the nonreciprocal emitters considered in this work [27], which consist of multiple thin InAs films and a reflective substrate, as shown in Figure 1b. Each layer of the structure would have a different carrier concentration to induce an ENZ effect at different wavelengths. To show the ENZ mode, we calculate the real part of permittivity of InAs layers with varying carrier concentration of n_{e1}, n_{e2}, n_{e3}, n_{e4}, and n_{e5}, which are 4×10^{17} cm^{-3}, 5×10^{17} cm^{-3}, 6×10^{17} cm^{-3}, 7×10^{17} cm^{-3}, and 8×10^{17} cm^{-3}, respectively. As shown in Figure 1c, when the carrier concentration increases from n_{e1} to n_{e5}, an obvious shift of the ENZ wavelengths occurs. We further calculate the contrast between absorptivity and emissivity for each InAs layer on top of a reflection substrate, and the results are shown in Figure 1d. The peak of the contrast occurs at the ENZ wavelengths, and therefore would shift with the carrier concentration increasing. Since each can have nonreciprocity at different narrow bands, building the multilayer structure consisting of InAs layers with different carrier concentrations to break Kirchhoff's law in broadband can be expected.

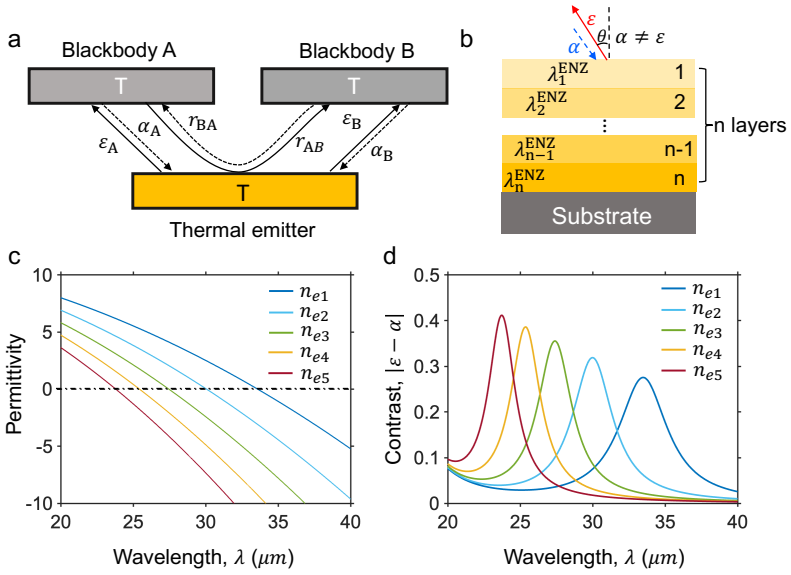

Figure 1 Nonreciprocal emitters that break Kirchhoff's law of radiation. (a) Schematic of a system consisting of a nonreciprocal thermal emitter and two blackbodies under thermal equilibrium, with the temperature of the thermal emitter the same as that of the blackbodies (b) Schematic of a gradient-doped multilayer structure for broadband nonreciprocal thermal emission, with each layer having a different carrier concentration and a different epsilon-near-wavelength that can break reciprocity at a specific wavelength range (c) The real part of permittivity of InAs layers with different carrier concentrations, i.e., n_{e1}, n_{e2}, n_{e3}, n_{e4}, and n_{e5}. (d) The contrast between absorptivity and emissivity of structures with a InAs layer on a reflection substrate, with the carrier concentration of the InAs layer ranging from n_{e1} to n_{e5}. The carrier concentration of n_{e1}, n_{e2}, n_{e3}, n_{e4}, and n_{e5} in (c) and (d) are 4×10^{17} cm^{-3}, 5×10^{17} cm^{-3}, 6×10^{17} cm^{-3}, 7×10^{17} cm^{-3}, and 8×10^{17} cm^{-3}, respectively, and the magnetic field is 1.5 T.

3 RESULTS AND DISCUSSIONS

To better compare our results with the state-of-the-art design, we first reproduce the results in Ref. [25] for a gradient multilayer structure of InAs with a linear doping profile, as shown in Figure 2. The

multilayer structure includes 10 layers of InAs on top of a 500 μm highly doped InAs substrate for reflection, and each layer has the same thickness of 350 nm. The doping concentration increases from the top layer to the bottom layer, from 4×10^{17} cm^{-3} to 8.5×10^{17} cm^{-3}, with an equal concentration difference of 0.5×10^{17} cm^{-3} between two adjacent layers. For such a structure, since each layer has a different carrier concentration, each layer can provide a strong Kirchhoff's law-breaking effect near its ENZ wavelength [24]. The emissivity and absorptivity of the 10-layer gradient structure between 20-40 μm are then calculated to show this breaking effect at the incident angle of 60°, and we consider TM waves in the calculation because there is no magneto-optical response for TE waves and the structure is reciprocal for TM waves [25]. As shown in Figure 2b, the emissivity and absorptivity differ in a broad wavelength range from 20 to 40 μm. Figure 2c shows the contrast between emissivity and absorptivity, and the largest contrast is 0.5 around the wavelength of 30 μm, demonstrating strong nonreciprocal behaviors.

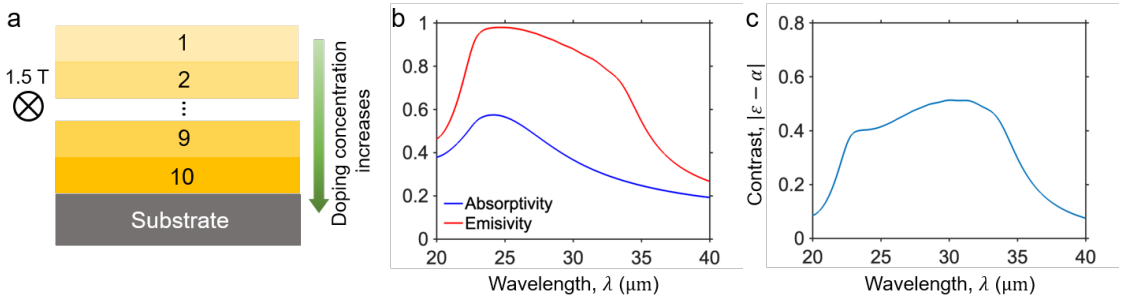

Figure 2 Nonreciprocal behavior of a 10-layer gradient doped InAs structure from Ref. [25]. (a) Schematic of the 10-layer gradient doped structure on top of a reflective substrate under a moderate magnetic field. Each layer has the same thickness, and the doping concentration increases from top to the bottom layer. (b) Emissivity and absorptivity of the 10-layer gradient structure at a magnetic field of 1.5 T and an incident angle of 60° (c) The contrast between the emissivity and absorptivity.

We now consider four different linear doping profiles inside the multilayer structure to investigate their effects on nonreciprocal behaviors. We still fix the number of layers to 10, the same as before, and use the same InAs substrate. Each layer has a thickness of 350 nm. In all these profiles, the doping concentration difference between the adjacent two layers is fixed to 0.5×10^{17} cm^{-3}, but the distribution of doping concentration is different, as shown in Figure 3a. For linear profile 1, 2, 3, and 4, the doping concentration increases from the top to the bottom, from the bottom to the top, from the two sides to the middle, and from the middle to the two sides, respectively. The contrasts between the emissivity and absorptivity of structures with different doping concentration profiles are shown in Figure 3b. Both the nonreciprocal bandwidth and the contrast change with the doping concentration profile. When the concentration increases from the top to the bottom, the structure has a larger nonreciprocal bandwidth, while the structure with the concentration increasing from the two sides to the middle has a slightly higher contrast between emissivity and absorptivity. For profiles 1 and 2, the carrier concentrations range from 4×10^{17} cm^{-3} to 8.5×10^{17} cm^{-3}, which is larger than that of profiles 3 and 4 (6×10^{17} cm^{-3} to 8.5×10^{17} cm^{-3}), and therefore they exhibit the nonreciprocal ENZ effect in a broader wavelength range.

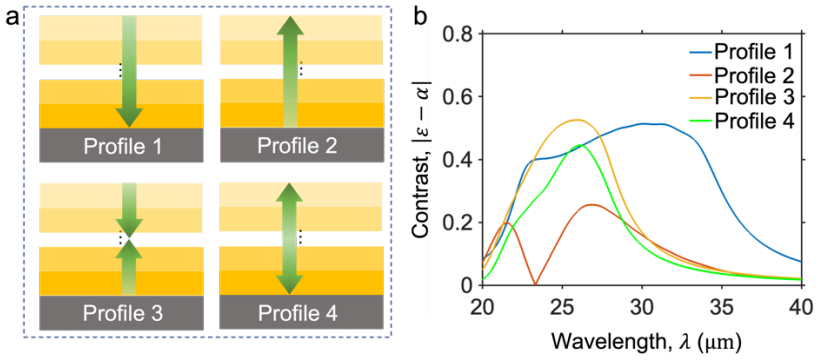

Figure 3 Nonreciprocal behavior of multilayer structures with different linear doping profiles. (a) Schematic of four different linear doping profiles inside the 10-layer gradient InAs structures, with the green arrow showing the increasing direction of the carrier concentration. For profile 1, 2, 3, and 4, the doping concentration ranges are $4 - 8.5 \times 10^{17}$ cm^{-3}, $4 - 8.5 \times 10^{17}$ cm^{-3}, $6 - 8.5 \times 10^{17}$ cm^{-3}, and $6 - 8.5 \times 10^{17}$ cm^{-3}, respectively. (b) The contrast between the emissivity and absorptivity of structures with four different linear doping profiles.

The broadband nonreciprocal behavior persists in a wide angler range. We plot the contrast between emissivity and absorptivity in the angular domain for all the above-discussed multilayer structures in Figure 4. It can be seen that the maximal contrast between emissivity and absorptivity occurs at an angle of around 60° for all the multilayer structures. Regardless of the differences in the nonreciprocal bandwidth, all the four different linear profiles could enable nonreciprocal absorptions and emissions across a broad angle, namely from 10° to 80°, making them omnidirectional nonreciprocal thermal emitters.

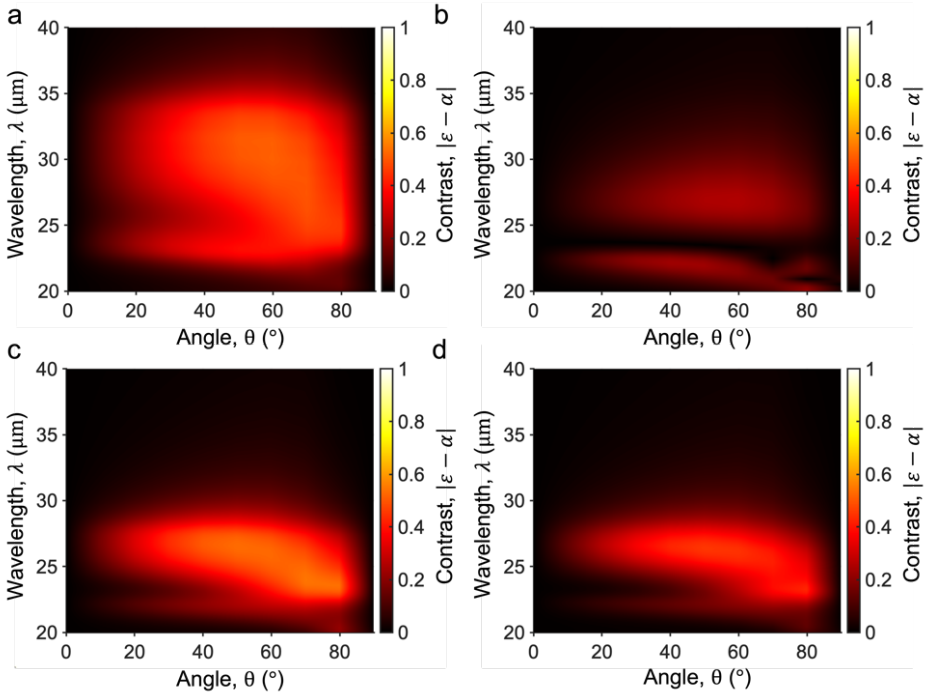

Figure 4 Angular distribution of the contrast between emissivity and absorptivity of multilayer structures with different linear doping profiles. (a) Profile 1, with the doping concentration increasing from the top to the bottom. (b) Profile 2, with the doping concentration increasing from the bottom

to the top. (c) Profile 3, with the doping concentration increasing from the two sides to the middle. (d) Profile 4, with the doping concentration increasing from the middle to the two sides.

The above analysis showcases the effectiveness of a gradually decreasing doping profile in terms of achieving broadband nonreciprocity. Built on this, we further investigate the case with a more generalized nonlinear doping profile [26], which can offer a higher tunability and may bring additional benefits. We still fix the number of layers to 10. As shown in Figure 5a, from the top to the bottom layer, the doping concentration (y) of each layer is set to be a function of the layer number (x), which ranges from 0 to 9. For the linear doping profile, y is proportional to x ($y{\sim}x$). While for nonlinear doping profiles, we choose two representative cases, i.e., y proportional to $x^{1/3}$ or x^3 (shown in Figure 5a). We fix the doping concentration of the top layer and bottom layer to be 4×10^{17} and 8.5×10^{17}, respectively, and the thickness is set to 350 nm for each layer.

The nonlinear doping profile indeed brings additional changes to the nonreciprocal performance. In Figure 5b, we calculate the contrast between emissivity and absorptivity of the three doping profiles, namely $y{\sim}x$, $y{\sim}x^3$, and $y{\sim}x^{1/3}$. It shows that the emitters in all the three cases have a broadband nonreciprocal behavior. The highest contrast is 0.6 achieved by the doping profile of $y{\sim}x^3$, which corresponds to a doping profile in which the doping concentration increases from the top layer to the bottom layer with increasing speed. A contrast of 0.6 is also the highest contrast under a moderate magnetic field (1.5 T) among all proposed multilayer nonreciprocal broadband emitters to the best of our knowledge. The multilayer structure with the nonlinear doping profile of $y{\sim}x^3$ also have a wide-angle nonreciprocal emission and absorption, as shown in Figure 5c, making it a broadband and wide-angle thermal emitter with high nonreciprocal performance. The proposed nonlinear doping profile with the highest nonreciprocal performance (red curve in Figure 5a) could be achieved by conventional ion implantation techniques that is well-established doping technologies in semiconductor industry [28, 29]. Another nonlinear doping profile (blue curve in Figure 5a) could be achieved using thermal-diffusion semiconductor doping technology [30, 31], which is also a well-developed technology in industrial semiconductor manufacturing featuring simplicity and affordability [32, 33]. Compared with the emitter with linear doping profile that requires epitaxially-grown multilayers[25], the emitter with nonlinear doping profile possess the advantages to be readily fabricated and widely applied while maintaining the high nonreciprocal performance.

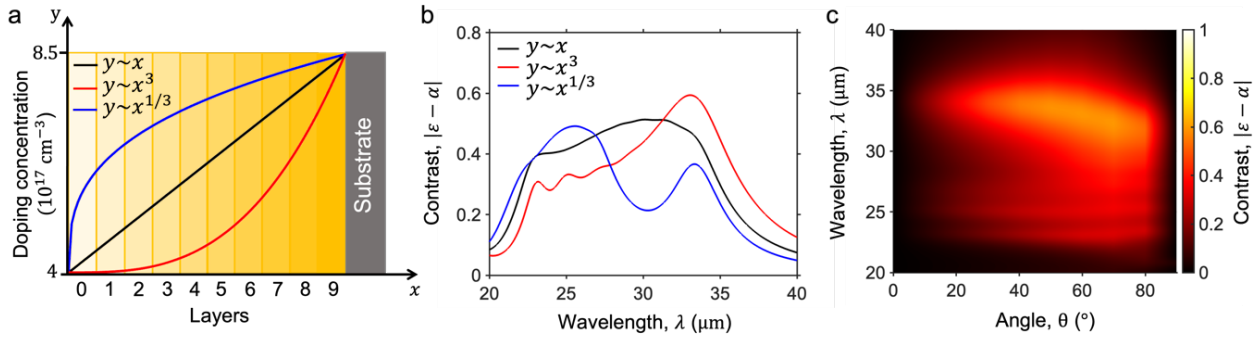

Figure 5 The difference between linear and nonlinear doping profiles inside the multilayer structure. (a) Schematic of different doping profiles inside the gradient multilayer structure, in which x is the number of layers and y is the doping concentration. (b) The contrasts between emissivity and absorptivity of multilayer structures with linear and nonlinear doping profiles. (c) Angular distribution of the contrast between emissivity and absorptivity of multilayer structures with nonlinear doping profile, $y{\sim}x^3$.

4 CONCLUSIONS

In conclusion, we reveal the effects of the ENZ profile on the nonreciprocal behaviors of broadband nonreciprocal multilayer emitters. Changing the ENZ profile can increase the contrast between the emissivity and absorptivity but leave the nonreciprocal bandwidth of such broadband nonreciprocal emitters unaffected. For InAs multilayer structures with different linear profiles, the multilayer structure has a broader nonreciprocal bandwidth when the doping concentration increases from the top to the bottom. Under a fixed doping concentration difference between the top and the bottom, a nonlinear doping profile can result in a larger contrast between emissivity and absorptivity as compared to the linear doping profile, while maintaining the broad nonreciprocal bandwidth. A high contrast of 0.6 is achieved by the nonlinear profile in this work, which is the highest contrast achieved under moderate magnetic field among broadband nonreciprocal multilayer emitters to the best of our knowledge. This work of controlling the profile can also be applied to other gradient multilayer structures for performance improvements, and such nonreciprocal emitters designed in this work has the great potential to be used in many thermal management systems and energy-based applications, for example, radiative cooling. Since the multilayer emitter in the work has a stronger emission than compared with the absorption in the mid-infrared wavelength range, it has a great potential to be applied in radiative-cooling systems to improve their performance.

ACKNOWLEDGEMENT

B.Z. acknowledges the start-up funding from the University of Houston. The authors are grateful for the support of the Research Computing Data Core at the University of Houston for assistance with the calculations carried out in this work.

REFERENCES

[1] Kirchhoff G. Über das Verhältnis zwischen dem Emissionsvermögen und dem Absorptionsvermögen der Körper für Wärme und Licht. Von Kirchhoff bis Planck: Theorie der Wärmestrahlung in Historisch-kritischer Darstellung. 1978:131-51.
[2] Planck M. The theory of heat radiation: Blakiston; 1914.
[3] Zhang ZM, Zhang ZM, Luby. Nano/microscale heat transfer: Springer; 2007.
[4] Buhara E, Ghobadi A, Khalichi B, Kocer H, Ozbay E. Mid-infrared adaptive thermal camouflage using a phase-change material coupled dielectric nanoantenna. Journal of Physics D: Applied Physics. 2021;54:265105.
[5] Weinstein LA, Loomis J, Bhatia B, Bierman DM, Wang EN, Chen G. Concentrating solar power. Chemical Reviews. 2015;115:12797-838.
[6] Du C, Zhao X, Qian X, Huang C, Yang R. Heat-Localized Solar Evaporation: Transport Processes and Applications. Nano Energy. 2022:108086.
[7] Yin X, Yang R, Tan G, Fan S. Terrestrial radiative cooling: Using the cold universe as a renewable and sustainable energy source. Science. 2020;370:786-91.
[8] Raman AP, Anoma MA, Zhu L, Rephaeli E, Fan S. Passive radiative cooling below ambient air temperature under direct sunlight. Nature. 2014;515:540-4.
[9] Zhao B, Guo C, Garcia CA, Narang P, Fan S. Axion-field-enabled nonreciprocal thermal radiation in Weyl semimetals. Nano letters. 2020;20:1923-7.
[10] Asadchy VS, Mirmoosa MS, Diaz-Rubio A, Fan S, Tretyakov SA. Tutorial on electromagnetic nonreciprocity and its origins. Proceedings of the IEEE. 2020;108:1684-727.
[11] Zhu L, Fan S. Near-complete violation of detailed balance in thermal radiation. Phys Rev B. 2014;90:220301.
[12] Ghalekohneh SJ, Zhao B. Nonreciprocal Solar Thermophotovoltaics. Physical Review Applied. 2022;18:034083.
[13] Park Y, Zhao B, Fan S. Reaching the ultimate efficiency of solar energy harvesting with a nonreciprocal multijunction solar cell. Nano Letters. 2021;22:448-52.
[14] Park Y, Omair Z, Fan S. Nonreciprocal Thermophotovoltaic Systems. ACS Photonics. 2022;9:3943-9.
[15] Fan L, Guo Y, Papadakis GT, Zhao B, Zhao Z, Buddhiraju S, et al. Nonreciprocal radiative heat transfer between two planar bodies. Phys Rev B. 2020;101:085407.

[16] Zhu L, Fan S. Persistent directional current at equilibrium in nonreciprocal many-body near field electromagnetic heat transfer. Physical review letters. 2016;117:134303.
[17] Tsurimaki Y, Qian X, Pajovic S, Han F, Li M, Chen G. Large nonreciprocal absorption and emission of radiation in type-I Weyl semimetals with time reversal symmetry breaking. Phys Rev B. 2020;101:165426.
[18] Zhao B, Shi Y, Wang J, Zhao Z, Zhao N, Fan S. Near-complete violation of Kirchhoff's law of thermal radiation with a 0.3 T magnetic field. Optics letters. 2019;44:4203-6.
[19] Shayegan KJ, Zhao B, Kim Y, Fan S, Atwater HA. Nonreciprocal infrared absorption via resonant magneto-optical coupling to InAs. Science Advances. 2022;8:eabm4308.
[20] Pajovic S, Tsurimaki Y, Qian X, Chen G. Intrinsic nonreciprocal reflection and violation of Kirchhoff's law of radiation in planar type-I magnetic Weyl semimetal surfaces. Phys Rev B. 2020;102:165417.
[21] Park Y, Asadchy VS, Zhao B, Guo C, Wang J, Fan S. Violating Kirchhoff's law of thermal radiation in semitransparent structures. ACS Photonics. 2021;8:2417-24.
[22] Zhang Z, Zhu L. Nonreciprocal thermal photonics for energy conversion and radiative heat transfer. Physical Review Applied. 2022;18:027001.
[23] Wu J, Qing YM. Wide-angle and broadband nonreciprocal thermal emitter with cascaded dielectric and Weyl semimetal grating structure. Appl Phys Lett. 2023;122:012203.
[24] Zhang Z, Zhu L. Broadband Nonreciprocal Thermal Emission. Physical Review Applied. 2023;19:014013.
[25] Liu M, Xia S, Wan W, Qin J, Li H, Zhao C, et al. Nonreciprocal thermal radiation in ultrathin magnetized epsilon-near-zero semiconductors. arXiv preprint arXiv:220304488. 2022.
[26] Xu D, Zhao J, Liu L. Near-field thermal radiation of gradient refractive index slab: Internal polaritons. Appl Phys Lett. 2021;119:141106.
[27] Guo C, Zhao B, Fan S. Adjoint Kirchhoff's law and general symmetry implications for all thermal emitters. Physical Review X. 2022;12:021023.
[28] Large L, Bicknell R. Ion-implantation doping of semiconductors. Journal of Materials Science. 1967;2:589-609.
[29] Larson LA, Williams JM, Current MI. Ion implantation for semiconductor doping and materials modification. Reviews of Accelerator Science and Technology. 2011;4:11-40.
[30] Zagozdzon-Wosik W, Wolfe J, Teng C. Doping of trench capacitors by rapid thermal diffusion. IEEE electron device letters. 1991;12:264-6.
[31] Peiner E, Schlachetzki A, Krüger D. Doping profile analysis in Si by electrochemical capacitance-voltage measurements. Journal of the Electrochemical Society. 1995;142:576.
[32] Seo J-H, Wu H, Mikael S, Mi H, Blanchard JP, Venkataramanan G, et al. Thermal diffusion boron doping of single-crystal natural diamond. Journal of Applied Physics. 2016;119:205703.
[33] Ho JC, Yerushalmi R, Jacobson ZA, Fan Z, Alley RL, Javey A. Controlled nanoscale doping of semiconductors via molecular monolayers. Nature materials. 2008;7:62-7.